Fish Detection Using Electrical Impedance Spectroscopy

Lukasz J. Nowak and Martin Lankheet

***Abstract*—Fish detection in shallow water conditions or close to the bottom poses specific challenges, which often can hardly be addressed using typical acoustical or optical means. This significantly limits the possibilities of fish population monitoring and the use of fish detection for optimizing fishing techniques in such environments. Here, we investigate the potential of electrical impedance spectroscopy (EIS) as a remote-sensing technique for fish detection, to address this issue. The approach utilizes a set of electrodes to generate a low-intensity alternating electric current through water and to measure the impedance. We conducted a number of experiments in which a fish was swimming in a glass tank. We measured changes in impedance at different frequencies, using different electrode arrangements, while simultaneously tracking the fish position with a pair of cameras. We also created numerical models of the experimental setup using the finite-element method. The results of simulations were compared to the experimental data to test the accuracy of predictions and to determine if such a model could be a useful tool for designing detection setups for specific environmental conditions. We measured the robustness of the system to the presence of air bubbles as a potential source of disturbances. Our results show a clear correlation between the observed drops in both real and imaginary parts of the measured impedance and the position of the fish. Model simulations showed qualitatively and quantitatively similar results, indicating that such models could be suitable for practical applications.**

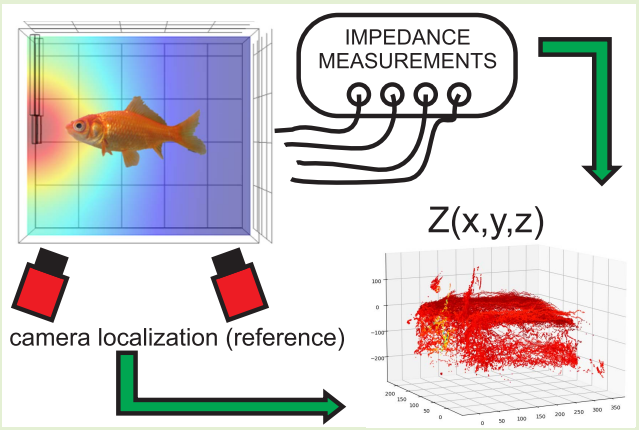

***Index Terms*—Electrical impedance, fish detection, remote sensing, spectroscopy.**

I. Introduction

A. Background

REMOTE-SENSING techniques for fish detection allow monitoring of population characteristics, behavior, and migration routes of various species, with minimal interference (see [1], [2], [3]). They can also serve to improve fishing techniques and minimize their ecological impact. In general, due to the relatively high propagation velocity and low attenuation of acoustic waves in water, ultrasound systems are usually the first choice in remote fish detection applications. This is especially true in open water reservoirs, where long detection ranges are required and background interference is minimal. The operation of such systems is based on the detection of ultrasound pulses reflected at boundaries of media with contrasting acoustical impedances, such as water and air. For this reason, fish with swim bladders are sources of particularly strong echo signals (see [1]). However, for the very same reason, acoustical means are very difficult or even impossible to implement in shallow and turbid environments, such as streams or fish ladders, with complex acoustic reflection patterns and very limited propagation lengths. It is also challenging to detect low-contrasting targets, such as flatfish on the seafloor with such systems, which would be particularly interesting in view of minimizing the ecological impact of bottom trawling [4].

Various visual observation techniques are also commonly employed for remote fish monitoring in a range of applications. They can be implemented by different means and at different scales. Fish counting by volunteers is a typical approach for monitoring population characteristics of various river species (see [5]). The method engages significant human resources and requires complex monitoring protocols (see [5]).

Manuscript received 22 August 2022; accepted 16 September 2022. Date of publication 26 September 2022; date of current version 31 October 2022. This work was supported by the Dutch Research Council (NWO), NWO Research Toward Sustainable Fisheries—Short-Term Innovation Projects under Grant 18527. The associate editor coordinating the review of this article and approving it for publication was Dr. Ravibabu Mulaveesala. *(Corresponding author: Lukasz J. Nowak.)*

This work involved human subjects or animals in its research. The authors confirm that all human/animal subject research procedures and protocols are exempt from review board approval.

The authors are with the Experimental Zoology Group, Department of Animal Sciences, Wageningen University & Research, 6708 PB Wageningen, The Netherlands (e-mail: lukasz.nowak@wur.nl).

Digital Object Identifier 10.1109/JSEN.2022.3207921

Optical fish detection can also be performed using cameras and image analysis software. Studies presented in the literature demonstrate reasonable accuracies achieved by such techniques, but their applicability is strongly limited by visibility conditions underwater (see [6], [7]). Other optical remote fish-sensing methods include utilization of satellite or airborne image datasets (see [8], [9]). This approach can provide unique large-scale results on fish distribution and is applicable for large water reservoirs and relatively low depth ranges.

In order to count fish in flowing waters, such as streams or fish passes, various techniques utilizing sensors implemented in specially designed tunnels or gates were developed [10]. This group includes also so-called "resistivity counters" or "impedance bridge fish counters," utilizing resistance measurements between a set of electrodes arranged parallelly across the water flow direction. A fish passing between the electrodes causes a measurable decrease in resistance, due to the higher electrical conductivity of tissues than the surrounding water [11]. Such systems were deployed in various water reservoirs and their readings were tested against results of visual observations [12], [13], [14], [15]. The comparisons revealed poor accuracy of resistivity counters, which significantly under- or overestimated the numbers of migrating fish [14], [15]. The studies conclude that the technique should be improved for the data to be useful for population monitoring.

The goal of the current study is to investigate mechanisms and phenomena underlying electrical impedance measurements as a remote fish-sensing technique in order to overcome some of the limitations of the approaches described above. We are particularly interested in close-range remote fish sensing at the bottom or in shallow waters. Such applications require electrode arrangement in a plane parallel to the desired detection volume, which presents significantly different challenges than in the cross-sectional case previously described in the literature. We have developed numerical models and compared their outcomes against the results of experiments conducted in controlled laboratory conditions. We developed and utilized an optical tracking system to provide reference data on fish locations. Such an approach allowed us to thoroughly study the relation between the detection system configuration, fish position, and impedance readings. We investigated both real and imaginary components of complex electrical impedance values in order to explore the potential of additional information carried by the phase shift between the voltage and current signals.

B. Electrical Impedance Measurements

We introduce a new approach to remote fish monitoring by analyzing electrical impedance values measured continuously with a submerged set of electrodes. Electrical impedance is a quantity relating measured voltage difference to the intensity of electric current flow between a set of electrodes, for a monochromatic harmonic signal. It is described with the following ratio:

$$Z = \frac{U_{\mathrm{PU}} \sin(\omega t)}{I_{\mathrm{CC}} \sin(\omega t + \theta)} \tag{1}$$

where Z is the impedance, U_{PU} is the amplitude of the voltage difference signal measured between the pickup (PU) electrodes, and I_{CC} is the amplitude of current intensity between the current-carrying (CC) electrodes. $\omega = 2\pi f$, where f is the electric signal frequency and θ is the phase difference between the voltage and current (see [16]). Separating PU and CC electrodes as independent pairs allows to mitigate the effects of interface impedance formed by an ionic double layer at the electrode surface in an electrolyte (see [17], [18]). We refer to such a case as a four-electrode configuration. If CC and PU electrodes are short-circuited to be a single electrode pair, we refer to it as a two-electrode configuration. Both arrangements were investigated in the current study.

Electrical impedance spectroscopy (EIS) is a measurement technique in which impedance values are determined over a range of frequencies of voltage/current signals. The results have a complex form

$$Z = \mathrm{Re}(Z) + j\,\mathrm{Im}(Z) \tag{2}$$

where $\mathrm{Re}(Z)$ is the real part of the impedance (resistance), $j = \sqrt{-1}$, and $\mathrm{Im}(Z)$ is the imaginary part (reactance). If the voltage is exactly in phase with the electric current, the impedance of the investigated object is purely resistive and $\mathrm{Im}(Z) = 0$. If there is a phase shift between the voltage and the current, then the impedance Z has either inductive character (with the current signal delayed relative to the voltage and $\mathrm{Im}(Z) > 0$) or capacitive character (voltage delayed, $\mathrm{Im}(Z) < 0$). Biological tissues typically have a purely capacitive character (see [18]). Here, we investigate independently both $\mathrm{Re}(Z)$ and $\mathrm{Im}(Z)$ within a discrete set of frequencies, in order to test how each is affected by the presence of a fish in the vicinity of the measurement electrodes. The signal amplitudes used in EIS are low (typically, up to 1–2 V, and below 10 mA), and the technique is thus harmless and imperceptible to animals, perhaps with the exception of electroreceptive species.

The impedance Z is a function of signal frequency, electrical properties of the medium, and geometrical arrangement of electrodes—their sizes, shapes, and mutual spatial orientation. Analytical formulas describing impedance are available only for a very limited number of specific cases, such as discrete electronic components or some very simple and regularly shaped conducing elements. In general, theoretical predictions are only possible based on numerical simulations and known electrical properties of the considered media.

EIS is commonly used in a range of scientific, biomedical, biological, and industrial applications. Examples include characterization of materials (see [16]), body composition analysis (see [19]), tumor detection (see [20]), and cytometry (see [21]). In relation to fish, this technique has been used to assess meat freshness and quality (see [22], [23], [24]). In the present study, we aim to investigate the possibilities of expanding the applicability range of EIS and characterize its potential for close-range remote fish sensing.

II. Materials and Methods

A. Experimental Investigations

Experimental measurements on remote detection of fish were conducted using the setup presented in Fig. 1. A single gold fish (*Carassius auratus*), with a body length of approximately 5 cm, was swimming freely in a glass tank

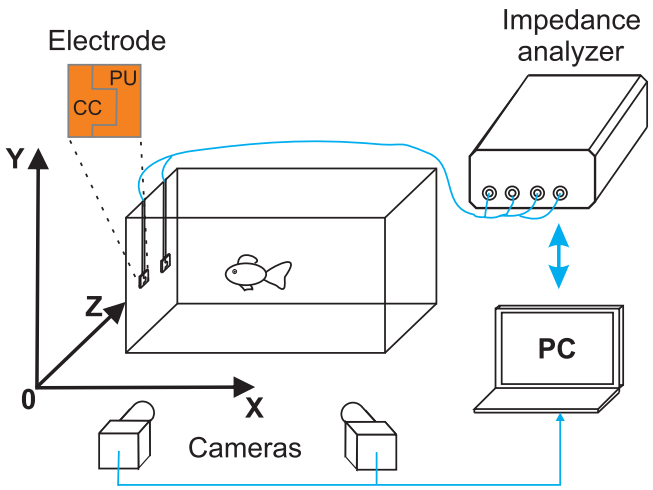

Fig. 1. Experimental setup and the adopted coordinate system.

filled with tap water at room temperature (20 °C). The inner tank dimensions were 400 × 240 × 295 mm in x-, y-, and z-directions, respectively (according to the coordinate system introduced in Fig. 1). The water level was approximately 225 mm and was checked on a daily basis. The fish was fed automatically three times a day and the light schedule was set to 12 h light and 12 h dark. The water in the aquarium was continuously filtered using a biological filter.

Impedance measurements were conducted using the MFIA impedance analyzer (Zurich Instruments, Switzerland). The data was continuously acquired from the analyzer at a sampling rate of 104 data points per second. The acquisition was performed using Python scripts communicating with the device's data server via a local network. Each data point included the determined real and imaginary impedance values and a time stamp.

The impedance analyzer was connected to two pairs of electrodes submerged in the tank. The electrodes were formed by copper layers on a standard 1.57-mm-thick glass-reinforced epoxy laminate printed circuit board substrate. Each pair consisting of one CC and one PU electrode was formed on a rectangular plate with dimensions 30 × 30 mm. The plate was separated into two parts of an equal area by grinding the copper layer between them, as illustrated in Fig. 1. When operating in the two-electrode configuration, the adjacent CC and PU electrodes were internally short-circuited by the impedance analyzer. The electrodes were submerged at identical depths of approximately 100 mm (center points distance to the surface). Three different spatial configurations were considered as follows.

1) Electrodes arranged along the z-direction, next to the tank wall at $x = 0$, and 166 mm apart (measured between their center points).
2) Same as above, but with the distance between electrodes equal to 45 mm.
3) Electrodes arranged along the x-direction, next to one of the longest tank walls, 100 mm apart from each other.

In all cases, the electrode surfaces were located 10 mm from the wall of the aquarium. The different electrode configurations enabled us to investigate the dependencies between the extent of the detection regions and the electrode arrangement.

An optical tracking system was used to provide reference data for the evaluation of the detection performance of the investigated approach. The fish position in the tank was continuously tracked with a synchronously triggered pair of monochromatic CCD cameras (Basler Ace 2048-90μm, Basler, Germany). Video images were captured at a frame rate of 50 Hz. The fish contour in each image was analyzed on-the-fly, using in-house developed Python scripts utilizing the OpenCV library. Fish contours and corresponding time stamps were saved to disk for the offline 3-D reconstruction of fish locations. To calculate fish location, we used the centroids of the contours for 3-D triangulation, based on 3-D calibration data for the camera setup. Calibrations took lens distortions, intrinsic and extrinsic camera parameters into account, and the results were verified based on known coordinates of identified markers.

The measurements were carried out for both two- and four-electrode configurations, three different spatial arrangements (as described above), and four signal frequencies of 1, 10, 50, and 100 kHz. For each combination of the system settings, both camera and impedance data were recorded. A single dataset for one setting obtained in this way covered a timespan of approximately 2–5 h. After finishing the experiments, while processing the results, it turned out that the data obtained for the two-electrode configuration, spacing 45 mm and frequency 1 kHz were corrupted and could not be used. However, due to a large amount of remaining, good-quality data covering all the other combinations this fact does not undermine the outcomes of the present study in any significant way.

The effect of air bubbles on impedance was determined using the four-electrode configuration, with electrodes arranged along the z-axis, 166 mm apart. One end of a silicone tubing was attached to an aluminum weight and put on the bottom of the tank, below and centrally to the electrodes. Several holes were cut in the submerged end of the tubing. Impedance measurements were carried out for different signal frequencies in the absence of the fish. During measurements, the air was blown by mouth through the tubing, in a cycle determined by respiratory rate. The air bubbles emerged to the surface, passing just in front of the electrode plane. Every single measurement (i.e., for each signal frequency) included 3600 data points, corresponding to approximately 35 s of acquisition time.

B. Data Postprocessing

The datasets of impedance values and fish coordinates for each corresponding configuration of system settings were combined based on timestamp values. The camera tracking data points were paired with the timewise closest impedance data points, restricting the allowed discrepancy to a maximum of 20 ms. If a pair could not be formed under this condition, the data point was discarded. In this way, every single measurement consisted of real and imaginary parts of the impedance together with the corresponding xyz location and timing data.

The variations in the measured impedance due to the presence of the fish in the vicinity of an electrode occurred on the background of a base impedance of water. Its value depends on all system parameters, including electrode spacing and configuration, signal frequency, and dimensions of the aquarium. It can also significantly fluctuate in time, showing changes over a period of minutes or hours much larger than those expected from the presence of a fish. Such relatively slow variations of base impedance values occur due to changes in the electric properties of water, caused, for example, by dissolving various substances. In laboratory conditions, these changes may be related to feeding, or the day–night light schedule affecting algae, fish physiology, and (bio)filter properties. We developed a dedicated algorithm to remove these slow variations in impedance and focus on changes due to the presence of the fish. The algorithm assumes that the impedance signatures of fish presence in the detection region occur in less than 45% of cases in the time-windowed data subsets. This assumption was well fulfilled in all the considered experimental results. The chosen time ratio value can also be adjusted to match different, specific conditions without any further changes to the algorithm itself. The filter procedure consisted of the following steps.

1) For each data point t_x, we define a time window ranging from $t_x - \Delta t$ to $t_x + \Delta t$ and we calculate the total range of measured values of real and imaginary impedance parts separately

$$Z_V^{\mathrm{Re}}(t_x) = \mathrm{abs}(\max(\mathrm{Re}(Z(t))) - \min(\mathrm{Re}(Z(t)))), \quad t \in < t_x - \Delta t; t_x + \Delta t)$$
$$Z_V^{\mathrm{Im}}(t_x) = \mathrm{abs}(\max(\mathrm{Im}(Z(t))) - \min(\mathrm{Im}(Z(t)))), \quad t \in < t_x - \Delta t; t_x + \Delta t).$$

2) Based on the distribution of signal variations in these time windows, we calculated threshold values as 55th percentiles of Z_V^{Re} and Z_V^{Im}. Intervals with variations below this limit are unlikely to contain detections and reflect the baseline.
3) For intervals below the variability limit, containing at least 50 data points, the baseline value was determined as the mean value for the interval.
4) For all other data points, the base impedance values were calculated using linear interpolation.

To obtain impedance variations due to fish presence irrespective of background variations, we subtracted the background level from the actual measurements. Baseline corrections were performed for the real and imaginary parts separately.

To analyze impedance values versus fish position for different cross-sectional planes or along different axes in the tank, we selected data points with a position margin equal to the electrode half-width (i.e., ±15 mm).

C. Numerical Simulations

We used numerical simulations to predict the sensitivity regions of the detection system in different electrode arrangements. The goal was to test whether simplified models based on fundamental phenomena underlying current flow between measurement electrodes are sufficient to characterize the system with reasonable accuracy. If predictions would agree with experimental results, modeling could constitute a valuable tool in designing and optimizing EIS-based fish detection systems for specific applications.

The numerical models were based on a finite-element method and implemented in COMSOL Multiphysics. We reproduced the 3-D geometry of the experimental setup, including the fish tank, electrodes, and electrode holders. The tank walls and air were assumed to constitute perfectly insulating boundary conditions. We used a four-electrode configuration, with one CC and one PU electrode pair, with shapes and dimensions as in the experimental setup. For each voxel, we calculated the sensitivity value, utilizing the principle of reciprocity (see [18], [25], [26])

$$S = \frac{\overrightarrow{J_{\mathrm{CC}}} \cdot \overrightarrow{J_{\mathrm{PU}}}}{I^2} \tag{3}$$

where $\overrightarrow{J_{\mathrm{CC}}} \cdot \overrightarrow{J_{\mathrm{PU}}}$ denotes a dot product of current density vectors induced by current flow I between CC and PU electrodes, respectively. The sensitivity S describes the contribution of resistivity of each voxel to the total measured impedance, which can be calculated using the following relation (see [18], [25], [26]):

$$Z = \iiint \rho S dV \tag{4}$$

where ρ denotes the resistivity of a volume element dV.

The model does not take into account the influence of fish presence on current density distribution and, consequently, impedance values, as such simulations would require individual calculations for every single case of fish size, effective electrical properties, spatial orientation, and location relative to the electrodes. Instead, sensitivity S distributions were calculated in a single run for each electrode arrangement in the tank. The results were used to predict the extent of regions in which fish presence would manifest itself by changes in the determined impedance values, as well as the relative range of these changes. For the sake of comparison with experimental results, the corresponding datasets were normalized.

III. Results

Fig. 2 presents the mean raw impedance values (before baseline correction) determined experimentally for all the tested system settings. The resistance values obtained with a two-electrode configuration are significantly higher compared to the results of four-electrode measurements. They also vary more with the signal frequency. These observations are consistent with the expected interface impedance effects. For comparing the different settings, it is obviously critical to correctly subtract the baseline levels.

Figs. 3 and 4 present two examples of merged impedance and localization data, with resistance and reactance values (before baseline correction) plotted versus time and fish coordinates. In both examples, the fish approaches the pair of electrodes, which induces clear reductions of impedance relative to a steady baseline level. The observed changes in real and imaginary impedance parts have a similar character, but

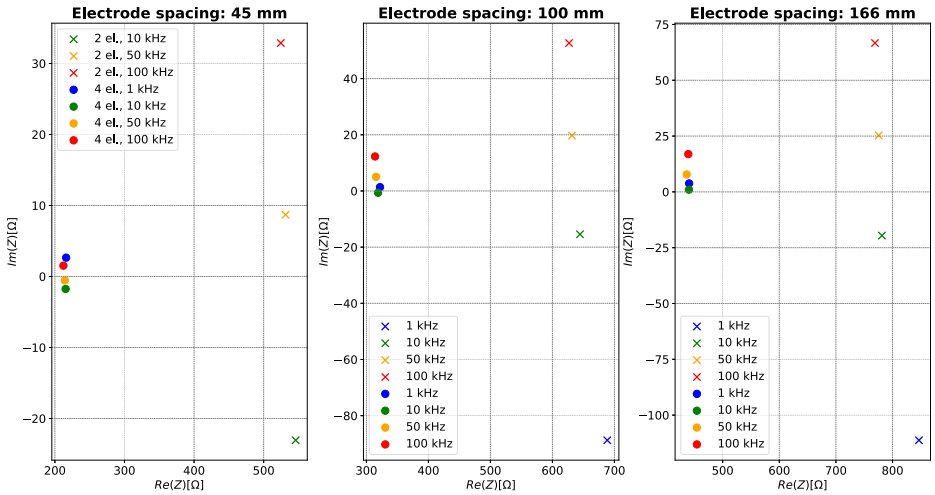

Fig. 2. Mean raw impedance values (before baseline correction) determined experimentally for different system settings.

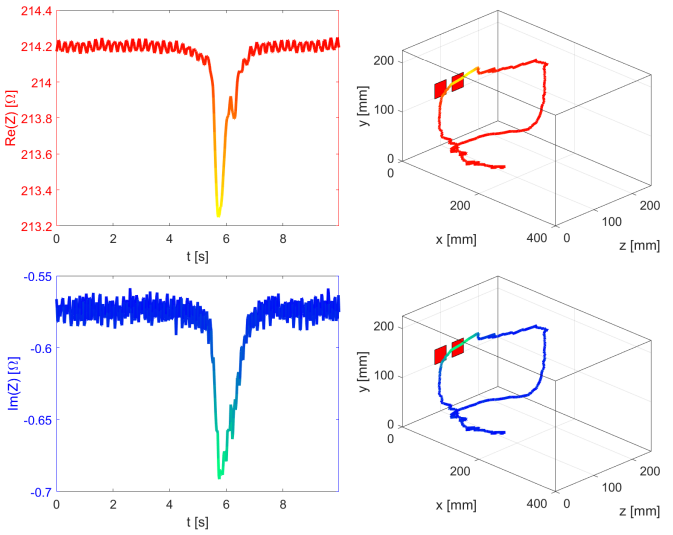

Fig. 3. Impedance values presented as functions of time (left), and fish coordinates in the tank (right; top—real part, bottom—imaginary part). Measurements performed using a four-electrode configuration, with a signal frequency of 50 kHz. Electrodes arranged along the *z*-direction, 45 mm apart.

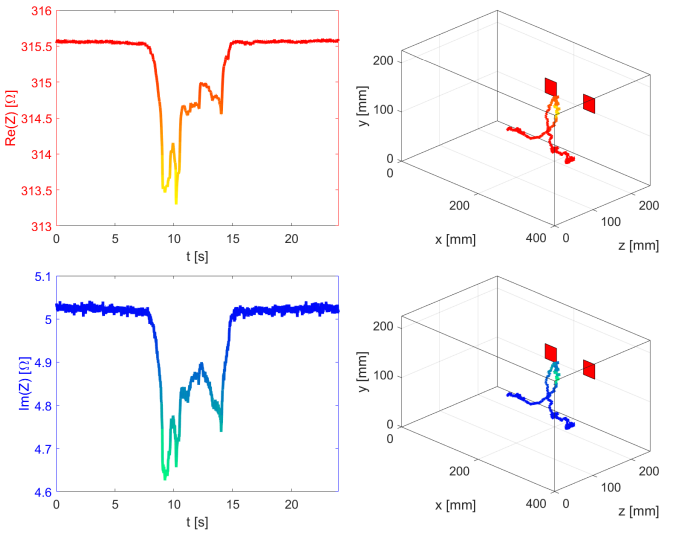

Fig. 4. Impedance values presented as functions of time (left), and fish coordinates in the tank (right; top—real part, bottom—imaginary part). Measurements performed using a four-electrode configuration, with a signal frequency of 50 kHz. Electrodes arranged along the *x*-direction, 100 mm apart.

differ in levels and scale. For all configurations and stimulus settings, we recorded at least 25 comparable events.

To compare the different configurations and settings, we calculated the median impedance deviations relative to the baseline, in a horizontal (xz) plane including the electrode center points (Figs. 5–7). Each figure compares resistance and reactance data for the two-electrode and four-electrode configurations, for different signal frequencies. Different spatial arrangements of the electrodes are presented in separate figures. Using median values, rather than means, mitigates the effects of extreme peaks caused by incidental contact of the fish with the electrodes. As the fish was swimming freely in the tank, the data coverage is not homogeneous and varies between the measurements. Still, due to the relatively long acquisition times, the results are conclusive and allow for comprehensive analysis and comparison of different settings.

In all the investigated cases, any significant changes in both resistance and reactance are observed only for fish positions in the vicinity of the measurement electrodes. Spatial distributions of deviations of real and imaginary impedance parts overlap in the corresponding measurements. All the observed changes related to the fish presence in the detection regions are declines in the determined values. Such an observation is in accordance with expectations, as fish tissue resistivity is lower than the surrounding water, and its dielectric properties are purely capacitive (see [22]). For electrodes relatively far apart, for example, 166 mm (Fig. 5) or 100 mm (Fig. 7), the sensitivity profiles show two separate peaks: one close to each PU electrode. For electrodes close together (45 mm, Fig. 6), the peaks tend to fuse to a single peak. The observed impedance distributions do not expose significant frequency dependencies in neither level nor their spatial extent within the considered signal bandwidth.

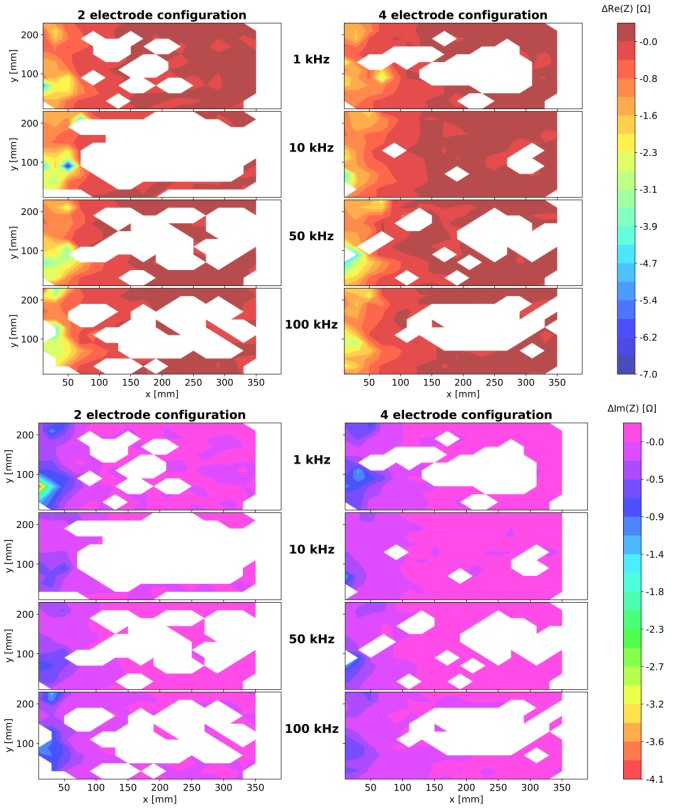

Fig. 5. Median resistance (top) and reactance (bottom) deviations in the *xz*-plane including electrode center points. Electrodes 166 mm apart, arranged centrally at $x = 0$.

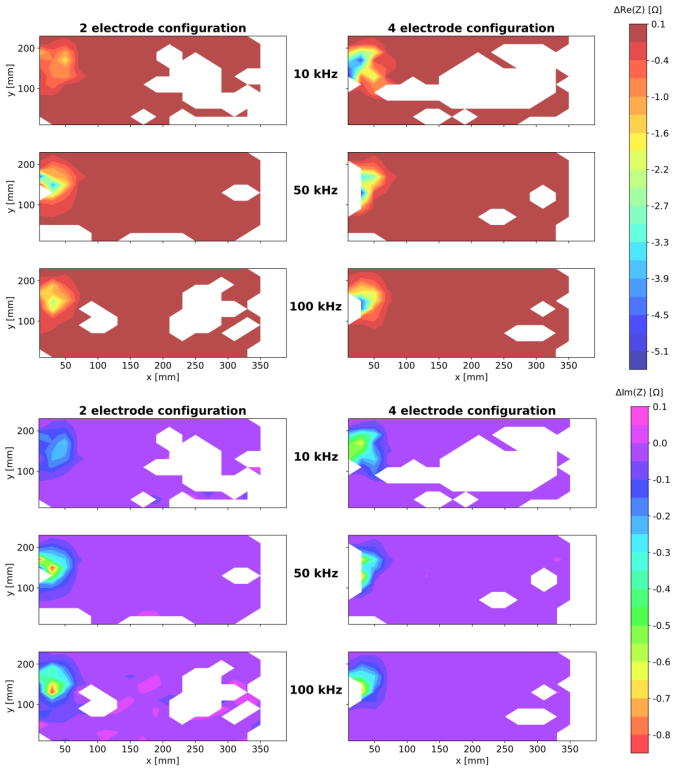

Fig. 6. Median resistance (top) and reactance (bottom) deviations in the *xz*-plane including electrode center points. Electrodes 45 mm apart, arranged centrally at $x = 0$.

In Fig. 8, we compare model sensitivity and experimental impedance values in the xz planes, including center points of the electrodes, similar to those presented in Figs. 5–7. To this end, both datasets were normalized to their maximum value in the time series. The results were obtained for electrodes arranged in the z-direction, 166 and 45 mm apart, for a four-electrode measurement configuration and 1-kHz signal frequency. The numerical predictions show high sensitivity regions just next to the electrodes and rapid decay with increasing distance. The experimental results show a very similar pattern, with a merged peak for the electrodes 45 mm apart and two clearly separate peaks for electrodes 166 mm apart. A similar fusion of peaks for electrodes place closely together was seen in Figs. 5–7. In Fig. 9, we compare measurements and model predictions in more detail, for the central axis perpendicular to the electrode plane. These line plots allow for a more detailed comparison in this region, putting aside the sensitivity hotspots just next to the electrode surfaces. In both configurations, the recordings show a range of values at similar distances from the electrodes, which presumably correspond to deviations from the line, within the selected margin limits. For a 45-mm electrode separation, some of the experimental data points show significant changes in measured impedance for fish positions several centimeters away from the predicted sensitivity region. This deviation, however, is within the size of the fish and may relate to the orientation of the fish, which causes a mismatch between the volume occupied by the fish, and the location of the fish centroid that was used to compare values to model simulations.

To characterize the detection performance of the investigated remote fish-sensing system, we determined receiver-operating characteristic (ROC) curves and calculated area under curve (AUC) values for all the investigated system settings. Based on the results of simulations and experiments we chose for this purpose, the extents of detection regions to be equal to electrode spacing + 2*electrode width along the electrode axis, 2*electrode width in the y-direction, and detection ranges from the electrode planes determined based on adopted sensitivity thresholds and results of simulations. Normalized sensitivity values along the central axes were considered, as illustrated in Fig. 9. Tables I and II present the results obtained for detection ranges corresponding to sensitivity thresholds equal to 0.01 and 0.1, respectively. The determined detection distances in the first case were equal to 54.28, 127.33, and 191.78 mm, for electrode spacing of 45, 100, and 166 mm, respectively. A tenfold increase in the sensitivity threshold (to 0, 1) resulted in a decrease of the corresponding distances to 32.16, 65.07, and 107.86 mm. Four different detection thresholding parameters were considered: resistance only (Re(Z)), reactance only (Im(Z)), logical conjunction of both (Re(Z) AND Im(Z)), and logical disjunction of both (Re(Z) OR Im(Z)). AUC values based on resistance values are generally higher than those for reactance values. Values based on the logical conjunction closely match those based on resistance values only and are in general higher than the results obtained for logical disjunction.

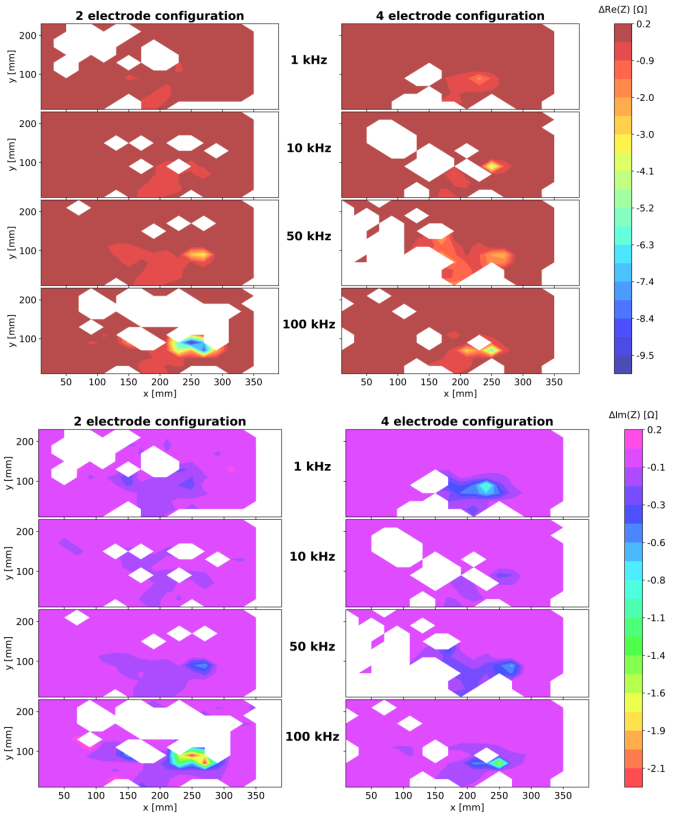

Fig. 7. Median resistance (top) and reactance (bottom) deviations in the *xz*-plane including electrode center points. Electrodes 100 mm apart, arranged centrally at $y = 0$.

Configuration with electrodes close together (45 mm) proved worst among the considered electrode arrangements, still reaching, in many cases, AUC values greater than 0.9. Moving electrodes further apart allows not only to significantly increase the expected detection distance (based on calculated sensitivity values along the central axis), but also results in improved detection performance. In terms of the signal frequency, the highest AUC values are generally achieved for the mid-frequency range in the considered bandwidth, that is, for 10 and 50 kHz.

Fig. 10 presents the results of impedance measurements, obtained while periodically blowing air bubbles in front of the electrodes. The bubbles were blown by mouth, following the respiratory rate. The moments of bubbles passing the electrodes are clearly visible in resistance plots as periodical increases of the base value. The changes are clear and significantly above the noise level in all the considered cases. The reactance plots show no such visible signatures of air bubbles' presence. The character of the observed deviations of impedance values is significantly different compared to the changes induced by the fish appearance in the detection region. This suggests that these two cases should be relatively simple to distinguish using the described remote-sensing system.

IV. Discussion

The results introduced in the present study indicate that electrical impedance measurements can be a useful and reliable tool for remote fish-sensing applications. The data presented in Figs. 3–7 show clearly that all the significant decreases in the resistance and reactance values correspond to fish positions in front and in the vicinity of the electrodes. High detection performance capabilities are also confirmed by the calculated AUC values, presented in Tables I and II.

Absolute measured impedance values depend on a number of factors, including electrode shapes and spatial arrangement, configuration, wiring, and electrical properties of water. The latter component can also fluctuate in time, as a result of, for example, the dissolution of various substances. Those slow changes can, in some cases, exceed the expected signatures of fish presence. For that reason, temporal impedance deviations instead of absolute values should be analyzed. We introduced an algorithm for calculating the resistance and reactance deviations from a slowly varying baseline, which proved efficient in our study. The algorithm utilizes backward- and forward-time windowing suitable for off-line analysis. It could, however, easily be converted for real-time detection by only taking earlier data points into account. Moreover, the results did not critically depend on the parameters of the filter, and other means of determining and discounting baseline fluctuations might work as well.

Absolute impedance values determined using the two-electrode configuration are significantly different from those obtained using the four-electrode configuration. The phenomenon is illustrated in Fig. 2. The resistance and reactance values are more than twice as high when CC and PU electrodes are short-circuited to form a single pair. This effect can be explained by electrode polarization and additional interface impedance [18]. The results obtained using a two-electrode configuration also show significantly higher frequency dependence than in the case of separated CC and PU electrodes. There are no distinct differences between the determined median impedance deviation values, as illustrated in Figs. 5–7. However, the changes relative to the absolute, baseline impedance values are greater for the four-electrode configurations. These observations lead to the conclusion that using separate CC and PU electrode pairs should be the preferred configuration for remote fish detection.

We investigated the detection performance for signal frequencies ranging from 1 to 100 kHz. Decreases in the determined AUC values can be observed in some cases at the extremes of the considered band, as illustrated in Tables I and II. Frequency has also a clear influence on the measured absolute impedance values. This effect can be seen in plots in Fig. 2. In general, the results indicate that the whole investigated frequency bandwidth can be considered useful for remote fish-sensing applications. Moreover, variations as a function of frequency could provide a more detailed impedance signature. This conclusion indicates possible directions for future research on, for example, using potential frequency dependencies to discriminate various objects in the detection region, or distinguishing individual fish species.

Although the results presented in Tables I and II indicate that resistance measurements alone should be sufficient to achieve high detection performance, further investigations on

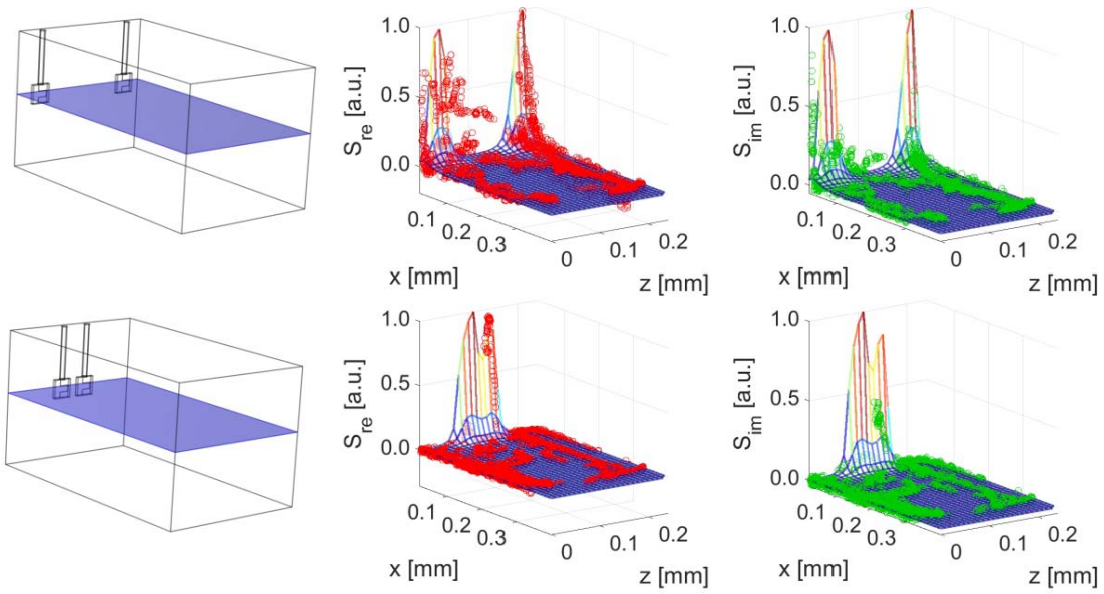

Fig. 8. Normalized sensitivity distributions determined numerically (color grids, right and in the middle) in the *xz* planes, compared to the normalized impedance deviations determined experimentally (red markers and middle column—real parts; green markers and right column—imaginary parts). Top row—electrodes 166 mm apart, bottom row—electrodes 45 mm apart. Sketches on the left illustrate the corresponding geometries and data planes.

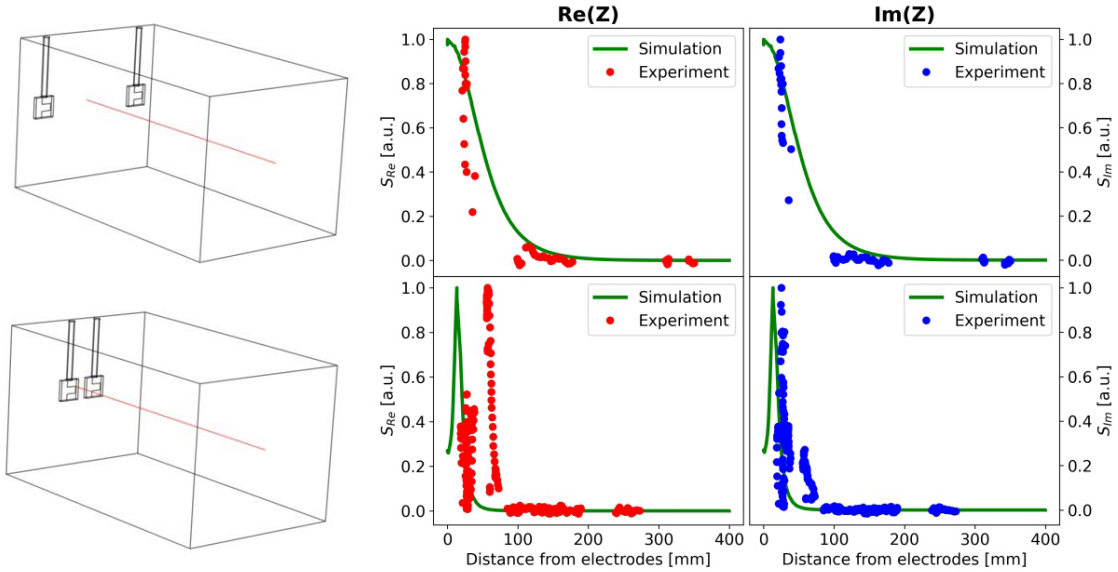

Fig. 9. Normalized sensitivity distributions determined numerically along the central electrode axes (line plots, right and in the middle), compared to the normalized impedance deviations determined experimentally (red markers and middle column—real parts; blue markers and right column—imaginary parts). Top row—electrodes 166 mm apart, bottom row—electrodes 45 mm apart. Sketches on the left illustrate the corresponding geometries.

the influence of air bubbles show clear benefits of employing both real and imaginary impedance parts for remote sensing of fish. Air bubbles are the primary obstacle for sonars and echo sounders. Being able to mitigate the effects related to their presence in the detection region could be one of the important advantages of the introduced approach over other remote-sensing means. As illustrated in Fig. 10, resistance values may be heavily affected by the presence of air bubbles. However, the imaginary part of the impedance is almost insensitive to bubbles, constituting a reliable discrimination criterion. Optimally combining resistance and reactance measurements may therefore provide a more robust signal for fish detection.

Numerical simulations could constitute a useful tool for optimization of an EIS-based fish detection system configuration for specific applications. We tested this approach by calculating spatial distributions of the sensitivity values defined with (3) for selected laboratory setup settings. Sensitivity S is defined for unit voxel elements and defines the contribution of a voxel to the overall measured impedance. The model that we used did not take the actual volume occupied by the

TABLE I

AUC VALUES CALCULATED FOR ALL THE INVESTIGATED SYSTEM SETTINGS. DETECTION RANGES WERE DETERMINED BASED ON NORMALIZED SENSITIVITY THRESHOLD EQUAL TO 0.01 AS 54.28, 127.33, AND 191.78 mm, FOR ELECTRODE SPACING 45, 100, AND 166 mm, RESPECTIVELY. FOUR DIFFERENT THRESHOLDING PARAMETERS ARE CONSIDERED: RESISTANCE ONLY (RE(z)), REACTANCE ONLY (IM(z)), LOGICAL CONJUNCTION OF BOTH (RE(z) AND IM(z)), AND LOGICAL DISJUNCTION OF BOTH (RE(z) OR IM(z))

Measurement Setup			**AUC**			
Electrode configuration		**Signal frequency**	**Re(Z)**	**Im(Z)**	**Re(Z) AND Im(Z)**	**Re(Z) OR Im(Z)**
Electrodes along Z direction, spacing 45 mm	2. electrode configuration	1 kHz	NA	NA	NA	NA
		10 kHz	0.8001	0.7355	0.8001	0.7358
		50 kHz	0.9289	0.9081	0.9289	0.9081
		100 kHz	0.8155	0.7546	0.8152	0.7551
	4. electrode configuration	1 kHz	0.5828	0.6208	0.6030	0.6176
		10 kHz	0.7101	0.6931	0.7095	0.6944
		50 kHz	0.9030	0.9016	0.9032	0.9015
		100 kHz	0.9320	0.8879	0.9328	0.8891
Electrodes along Z direction, spacing 166 mm	2. electrode configuration	1 kHz	0.8526	0.8228	0.8229	0.8544
		10 kHz	0.9619	0.9138	0.9614	0.9319
		50 kHz	0.8754	0.8675	0.8674	0.8755
		100 kHz	0.7662	0.7010	0.7645	0.7038
	4. electrode configuration	1 kHz	0.8225	0.7731	0.8221	0.7752
		10 kHz	0.8659	0.8462	0.8657	0.8465
		50 kHz	0.9304	0.9185	0.9303	0.9184
		100 kHz	0.8361	0.7812	0.8361	0.7811
Electrodes along X direction, spacing 100 mm	2. electrode configuration	1 kHz	0.9939	0.7859	0.9941	0.7859
		10 kHz	0.9549	0.8678	0.9409	0.9662
		50 kHz	0.9753	0.9443	0.9753	0.9444
		100 kHz	0.9315	0.7197	0.9315	0.7295
	4. electrode configuration	1 kHz	0.9502	0.8717	0.8985	0.9520
		10 kHz	0.9806	0.9802	0.9807	0.9802
		50 kHz	0.9923	0.9896	0.9919	0.9926
		100 kHz	0.8844	0.7924	0.8850	0.7997

TABLE II

AUC VALUES CALCULATED FOR ALL THE INVESTIGATED SYSTEM SETTINGS. DETECTION RANGES WERE DETERMINED BASED ON NORMALIZED SENSITIVITY THRESHOLD EQUAL TO 0.1 AS 32.16, 65.07, AND 107.86 mm, FOR ELECTRODE SPACING 45, 100, AND 166 mm, RESPECTIVELY. FOUR DIFFERENT THRESHOLDING PARAMETERS ARE CONSIDERED: RESISTANCE ONLY (RE(z)), REACTANCE ONLY (IM(z)), LOGICAL CONJUNCTION OF BOTH (RE(z) AND IM(z)), AND LOGICAL DISJUNCTION OF BOTH (RE(z) OR IM(z))

Measurement Setup			**AUC**			
Electrode configuration		**Signal frequency**	**Re(Z)**	**Im(Z)**	**Re(Z) AND Im(Z)**	**Re(Z) OR Im(Z)**
Electrodes along Z direction, spacing 45 mm	2. electrode configuration	1 kHz	NA	NA	NA	NA
		10 kHz	0.7311	0.6493	0.7312	0.6491
		50 kHz	0.9200	0.8905	0.9201	0.8905
		100 kHz	0.8819	0.7897	0.8807	0.7903
	4. electrode configuration	1 kHz	0.5844	0.6313	0.6118	0.6246
		10 kHz	0.6414	0.6250	0.6410	0.6264
		50 kHz	0.7628	0.7794	0.7632	0.7793
		100 kHz	0.9327	0.8517	0.9344	0.8521
Electrodes along Z direction, spacing 166 mm	2. electrode configuration	1 kHz	0.9369	0.8951	0.8951	0.9391
		10 kHz	0.9712	0.9233	0.9705	0.9419
		50 kHz	0.9607	0.9534	0.9534	0.9606
		100 kHz	0.8973	0.7995	0.8965	0.8034
	4. electrode configuration	1 kHz	0.9281	0.8932	0.9276	0.8960
		10 kHz	0.9388	0.9179	0.9386	0.9183
		50 kHz	0.9648	0.9556	0.9646	0.9556
		100 kHz	0.9244	0.8555	0.9244	0.8553
Electrodes along X direction, spacing 100 mm	2. electrode configuration	1 kHz	0.9968	0.8083	0.9970	0.8083
		10 kHz	0.9948	0.8782	0.9750	0.9930
		50 kHz	0.9913	0.9644	0.9913	0.9644
		100 kHz	0.9536	0.7305	0.9529	0.7412
	4. electrode configuration	1 kHz	0.9947	0.9925	0.9948	0.9952
		10 kHz	0.9956	0.9944	0.9956	0.9944
		50 kHz	0.9983	0.9983	0.9983	0.9983
		100 kHz	0.9869	0.8588	0.9868	0.8664

fish into account. Because we compare model voxel values to fish centroid coordinates, deviations are to be expected due to the size and orientation of the fish. A better match might be obtained by taking all the voxels into account that the fish body occupies. Still, this would be a rough estimate only because in modeling the electric fields, we did not take into account the

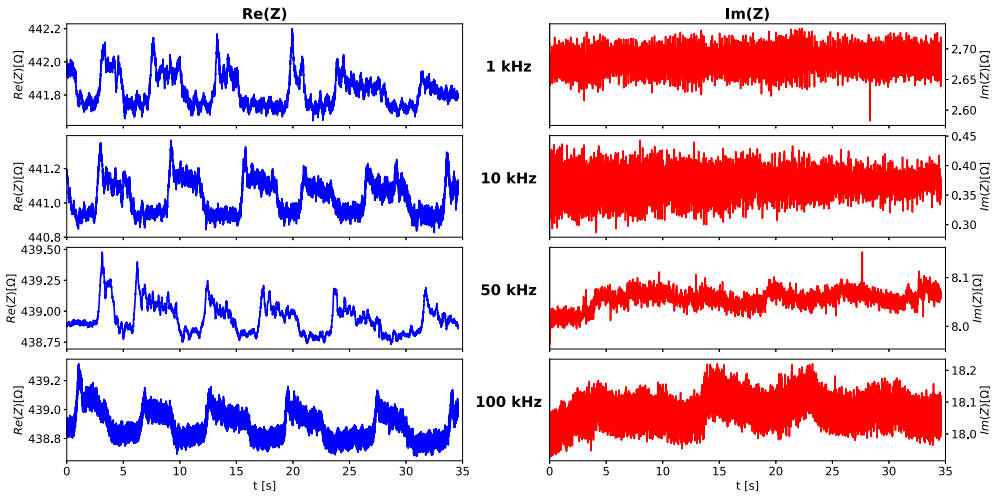

Fig. 10. Real and imaginary parts of impedance values versus time, determined for different signal frequencies while periodically blowing air bubbles in front of the electrodes.

influence of a fish's presence on current distribution, which is expected to be significant. However, if a fish would be included in the simulations, then spatial distributions could only be calculated by sweeping its position and orientation in a 3-D space, and performing independent analysis for each step. Such an approach would be far more computationally expensive than the introduced model, and it would require estimates of the impedance values of fish tissues. The results of our investigations, illustrated in Figs. 8 and 9, show that despite the simplifications that we applied, the proposed solution ensures reasonable accuracy and should prove useful in designing optimal remote-sensing configurations.

The experimental results show that a useful detection range of the described remote-sensing system, with electrodes arranged in a single plane, is at least equal to the electrode spacing for a fish size of approximately 5 cm. In this region, the ROC analysis and resulting AUC values show, in most cases, high detection performance. This, of course, corresponds to the high signal-to-noise ratios for recorded impedance values. Obviously, the shape and size of the detection volume will depend on electrode configuration, which is also illustrated by both experimental results and model simulations. A more general and accurate estimate for the volume in which fish are detectable could be deduced from model simulations, in combination with reasonable estimates of noise in the measurements. Model simulations, therefore, can also indicate how to adopt the electrode arrangements for minimal detection coverage in a specific practical application. The electrode arrangements that we used could, for example, be useful for fish counting in shallow passages, such as fish ladders. Electrodes situated at the bottom and facing upward could detect passing animals. In such cases, the limited detection range could actually be an advantage, as it would enable to avoid detection events and noise sources originating outside the region of interest (e.g., at the water surface).

The presented results of experiments and numerical simulations consider only a case with a single fish appearing at a time in the detection region. This allowed us to focus on fundamental phenomena underlying the operation of the investigated system and significantly simplified the requirements imposed on the optical tracking system used for reference. The observed drops in measured impedance values due to the fish presence in the vicinity of electrodes occur due to the contrast in electrical properties of the fish tissues and the surrounding water. It is thus expected that multiple fish individuals present simultaneously in the detection region would also cause observable decay in resistance and reactance values. Determining how many animals were detected would be a challenging task in the described system configuration, as the extent of the impedance drop itself does not allow us to draw such a conclusion. It might as well be related to fish size or distance to the electrodes. Still, it is not excluded that some detailed analysis of signal changes in time would enable us to distinguish at least some of such cases. The corresponding algorithm would most likely have to incorporate some additional data related to a given application, such as, for example, information about electrode movement in fishing gear or water current velocity in a stream or river. It is thus a topic for follow-up research aimed at specific implementations.

The promising outcomes of the presented results of experimental investigations conducted in laboratory conditions pave the way for further research aimed at practical applications of the introduced technique. The described studies should continue in various real-world conditions, taking into account different water compositions (including sea water), the presence of bottom sediments, and different objects typically encountered in water environments (plants, animals, and rocks). Characteristic signal signatures associated with various scenarios should be identified, and appropriate data-processing algorithms should be developed—possibly involving deep-learning techniques. Yet another direction for further research related to the present study is the exploitation of possibilities of expanding sensing capabilities by adding more independent electrode pairs. Combining time and spatial information could potentially enable us to, for example, estimate fish size or

distinguish signals originating from single or multiple fish individuals.

ACKNOWLEDGMENT

Lukasz J. Nowak would like to acknowledge Dr. Michal Penkowski from the Medical University of Gdansk for inspiration and advice.

REFERENCES

[1] D. N. MacLennan and E. J. Simmonds, *Fisheries Acoustics* (Fish & Fisheries Series), no. 5. Dordrecht, The Netherlands: Springer, 1992, doi: 10.1007/978-94-017-1558-4.

[2] N. O. Handegard, R. Patel, and V. Hjellvik, "Tracking individual fish from a moving platform using a split-beam transducer," *J. Acoust. Soc. Amer.*, vol. 118, no. 4, pp. 2210–2223, Oct. 2005. [Online]. Available: https://asa.scitation.org/doi/full/10.1121/1.2011410

[3] H. Balk and T. Lindem, "Improved fish detection in data from split-beam sonar," *Aquatic Living Resour.*, vol. 13, no. 5, pp. 297–303, Sep. 2000. [Online]. Available: https://www.cambridge.org/core/journals/aquatic-living-resources/article/abs/improved-fish-detection-in-data-from-splitbeam-sonar/CC85E15B85571D9A8539B628A1822D49

[4] P. Boute, "Effects of electrical stimulation on marine organisms," Ph.D. thesis, Dept. Animal Sci., Wageningen Univ. Res., Wageningen, The Netherlands, 2022.

[5] K. H. Bieluch, T. Willis, J. Smith, and K. A. Wilson, "The complexities of counting fish: Engaging citizen scientists in fish monitoring," *Maine Policy Rev.*, vol. 26, no. 2, pp. 1–11, Jan. 2017. [Online]. Available: https://par.nsf.gov/biblio/10103976-complexities-counting-fish-engaging-citizen-scientists-fish-monitoring

[6] C. Spampinato, Y.-H. Chen-Burger, G. Nadarajan, and R. Fisher, "Detecting, tracking and counting fish in low quality unconstrained underwater videos," in *Proc. 3rd Int. Conf. Comput. Vis. Theory Appl. (VISAPP)*, 2008, pp. 514–519. [Online]. Available: https://www.research.ed.ac.uk/en/publications/detecting-tracking-and-counting-fish-in-low-quality-unconstrained

[7] M.-C. Chuang, J.-N. Hwang, K. Williams, and R. Towler, "Tracking live fish from low-contrast and low-frame-rate stereo videos," *IEEE Trans. Circuits Syst. Video Technol.*, vol. 25, no. 1, pp. 167–179, Jan. 2015.

[8] D. Tonolla, C. Wolter, T. Ruhtz, and K. Tockner, "Linking fish assemblages and spatiotemporal thermal heterogeneity in a river-floodplain landscape using high-resolution airborne thermal infrared remote sensing and *in-situ* measurements," *Remote Sens. Environ.*, vol. 125, pp. 134–146, Aug. 2012. [Online]. Available: https://www.sciencedirect.com/science/article/abs/pii/S003442571200288X

[9] A. Knudby, E. LeDrew, and A. Brenning, "Predictive mapping of reef fish species richness, diversity and biomass in Zanzibar using IKONOS imagery and machine-learning techniques," *Remote Sens. Environ.*, vol. 114, no. 6, pp. 1230–1241, Jun. 2010. [Online]. Available: https://www.sciencedirect.com/science/article/abs/pii/S0034425710000295

[10] D. Li *et al.*, "Automatic counting methods in aquaculture: A review," *J. World Aquaculture Soc.*, vol. 52, no. 2, pp. 269–283, Apr. 2021. [Online]. Available: https://onlinelibrary.wiley.com/doi/pdf/10.1111/jwas.12745

[11] K. L. Liscom and C. D. Volz, "Impedance bridge fish counter," *Progressive Fish-Culturist*, vol. 37, no. 1, pp. 39–42, Jan. 1975. [Online]. Available: https://afspubs.onlinelibrary.wiley.com/doi/abs/10.1577/1548-8659%281975%2937%5B39%3AIBFC%5D2.0.CO%3B2

[12] D. A. Dunkley and W. M. Shearer, "An assessment of the performance of a resistivity fish counter," *J. Fish Biol.*, vol. 20, no. 6, pp. 717–737, Jun. 1982. [Online]. Available: https://onlinelibrary.wiley.com/doi/abs/10.1111/j.1095-8649.1982.tb03982.x

[13] D. G. Reddin, M. F. O'Connell, and D. A. Dunkley, "Assessment of an automated fish counter in a Canadian river," *Aquaculture Res.*, vol. 23, no. 1, pp. 113–121, Jan. 1992. [Online]. Available: https://onlinelibrary.wiley.com/doi/abs/10.1111/j.1365-2109.1992.tb00601.x

[14] I. P. Smith, A. D. F. Johnstone, and D. A. Dunkley, "Evaluation of a portable electrode array for a resistivity fish counter," *Fisheries Manag. Ecol.*, vol. 3, no. 2, pp. 129–141, Jun. 1996. [Online]. Available: https://onlinelibrary.wiley.com/doi/abs/10.1111/j.1365-2400.1996.tb00137.x

[15] J. J. Sheppard and M. S. Bednarski, "Utility of single-channel electronic resistivity counters for monitoring river herring populations," *North Amer. J. Fisheries Manag.*, vol. 35, no. 6, pp. 1144–1151, Nov. 2015. [Online]. Available: https://afspubs.onlinelibrary.wiley.com/doi/abs/10.1080/02755947.2015.1084407

[16] E. Barsoukov and J. R. Macdonald, Eds., *Impedance Spectroscopy: Theory, Experiment, and Applications*, 2nd ed. Hoboken, NJ, USA: Wiley, Mar. 2005.

[17] P. Kassanos, "Bioimpedance sensors: A tutorial," *IEEE Sensors J.*, vol. 21, no. 20, pp. 22190–22219, Oct. 2021.

[18] S. Grimnes and O. G. Martinsen, *Bioimpedance and Bioelectricity Basics*. New York, NY, USA: Academic, Aug. 2014.

[19] M. S. Mialich, J. M. F. Sicchieri, and A. A. J. Junior, "Analysis of body composition: A critical review of the use of bioelectrical impedance analysis," *Int. J. Clin. Nutrition*, vol. 2, no. 1, pp. 1–10, Jan. 2014. [Online]. Available: https://www.sciencedirect.com/science/article/pii/S0956566320307958

[20] M. Assenheimer *et al.*, "The T-SCANTMtechnology: Electrical impedance as a diagnostic tool for breast cancer detection," *Physiol. Meas.*, vol. 22, no. 1, pp. 1–8, Feb. 2001, doi: 10.1088/0967-3334/22/1/301.

[21] D. S. de Bruijn, P. M. T. Braak, D. B. Van de Waal, W. Olthuis, and A. van denBerg, "Coccolithophore calcification studied by single-cell impedance cytometry: Towards single-cell PIC:POC measurements," *Biosensors Bioelectron.*, vol. 173, Feb. 2021, Art. no. 112808. [Online]. Available: https://www.sciencedirect.com/science/article/pii/S0956566320307958

[22] J. Niu and J. Y. Lee, "A new approach for the determination of fish freshness by electrochemical impedance spectroscopy," *J. Food Sci.*, vol. 65, no. 5, pp. 780–785, Aug. 2000. [Online]. Available: https://onlinelibrary.wiley.com/doi/abs/10.1111/j.1365-2621.2000.tb13586.x

[23] X. Zhao, H. Zhuang, S.-C. Yoon, Y. Dong, W. Wang, and W. Zhao, "Electrical impedance spectroscopy for quality assessment of meat and fish: A review on basic principles, measurement methods, and recent advances," *J. Food Qual.*, vol. 2017, Jul. 2017, Art. no. e6370739. [Online]. Available: https://www.hindawi.com/journals/jfq/2017/6370739/

[24] J. Sun, R. Zhang, Y. Zhang, G. Li, and Q. Liang, "Estimating freshness of carp based on EIS morphological characteristic," *J. Food Eng.*, vol. 193, pp. 58–67, Jan. 2017. [Online]. Available: https://www.sciencedirect.com/science/article/pii/S0260877416302874

[25] F.-J. Pettersen and J. O. Høgetveit, "From 3D tissue data to impedance using simpleware ScanFE+IP and COMSOL multiphysics—A tutorial," *J. Electr. Bioimpedance*, vol. 2, no. 1, pp. 13–32, Apr. 2011. [Online]. Available: https://www.sciendo.com/article/10.5617/jeb.173

[26] M. Amini, H. Kalvøy, and Ø. Martinsen, "Finite element simulation of the impedance response of a vascular segment as a function of changes in electrode configuration," *J. Electr. Bioimpedance*, vol. 11, no. 1, pp. 112–131, Dec. 2020. [Online]. Available: https://www.ncbi.nlm.nih.gov/pmc/articles/PMC7851985/

Lukasz J. Nowak received the Ph.D. degree in electronics from the Institute of Fundamental Technological Research, Polish Academy of Sciences, Warsaw, Poland, in 2014, where he also led several research projects in the fields of biomedical acoustics, underwater communication, and active vibroacoustic control.

He is a Postdoctoral Researcher at Wageningen University & Research, Wageningen, The Netherlands, where he works on the development of fish detection means based on electrical impedance measurements. Before his current occupation, he worked at the University of Twente, Enschede, The Netherlands, studying mechanisms of interaction of light and sound in optically scattering media and developing acousto-optic imaging systems.

Martin Lankheet received the Ph.D. degree in neurophysiology from Helmholtz Institute, Utrecht University, Utrecht, The Netherlands, in 1990.

He is an Associate Professor at Wageningen University & Research, Wageningen, The Netherlands. He works on fish detection, biomechanics of fish swimming, insect flight, and sensory-motor control. He has led a wide range of projects in sensory physiology, visual perception, electroreception, directional hearing, and the effects of electrical pulsing in bottom trawling.